A simple penalty that encourages local invertibility and considers sliding effects for respiratory motion

Se Young Chun[a], Jeffrey A. Fessler[a] and Marc L. Kessler[b]

[a]Electrical Engineering and Computer Science,
[b]Radiation Oncology,
The University of Michigan, Ann Arbor, MI

ABSTRACT

Nonrigid image registration is a key tool in medical imaging. Because of high degrees of freedom in nonrigid transforms, there have been many efforts to regularize the deformation based on some reasonable assumptions. Especially, motion invertibility and local tissue rigidity have been investigated as reasonable priors in image registration. There have been several papers on exploiting each constraint separately.

These constraints are reasonable in respiratory motion estimation because breathing motion is invertible and there are some rigid structures such as bones. Using both constraints seems very attractive in respiratory motion registration since using invertibility prior alone usually causes bone warping in ribs. Using rigidity prior seems natural and straightforward. However, the "sliding effect" near the interface between rib cage and diaphragm makes problem harder because it is not locally invertible. In this area, invertibility and rigidity priors have opposite forces.

Recently, we proposed a simple piecewise quadratic penalty that encourages the local invertibility of motions. In this work we relax this penalty function by using a Geman-type function that allows the deformation to be piecewise smooth instead of globally smooth. This allows the deformation to be discontinuous in the area of the interface between rib cage and diaphragm. With some small sacrifice of regularity, we could achieve more realistic discontinuous motion near diaphragm, better data fitting error as well as less bone warping. We applied this Geman-type function penalty only to the x- and y-direction partial derivatives of the z-direction deformation to address the sliding effect. $192 \times 128 \times 128$ 3D CT inhale and exhale images of a real patient were used to show the benefits of this new penalty method.

Keywords: nonrigid image registration, piecewise smooth deformation, B-spline, bone rigidity, Geman function, regularization method

1. INTRODUCTION

Nonrigid image registration provides more flexible image matching but suffers by its ill-posedness and resulting in unrealistic deformations.[1] There has been lots of research on regularizing or constraining deformations with reasonable prior information such as smoothness of deformations, motion invertibility and tissue rigidity.

Motion invertibility constraint has been one of the reasonable constraints, but ensuring it has been challenging and computationally expensive. Since it is challenging to enforce motion inversibility on the continuous domain, there have been some relaxations of the problem for practical implementations: 1) enforcing motion invertibility only at discrete spatial points instead of on continuous image domain,[2,3] 2) using simpler deformation models such as linear deformations,[4,5] and 3) using simple, but restricted sufficient conditions .[6–8]

Tissue rigidity constraint has been another reasonable constraint in nonrigid image registration.[9–12] Some medical imaging modalities provide tissue rigidity information that can be incorporated well into the tissue rigidity constraint.

In respiratory motion image registration, it is natural to apply both invertibility and tissue rigidity constraints since respiratory motion is invertible - cycle of inhale and exhale - and there are some rigid structure such as bones. However,

This work was supported in part by NIH/NCI grant 1P01 CA87634 and P01 CA59827.
Se Young Chun: E-mail: delight@umich.edu, Telephone: 734 615 5735
Jeffrey A. Fessler: fessler@umich.edu, Telephone: 734 763 1434
Marc L. Kessler: mkessler@umich.edu, Telephone: 734 936 3592

Medical Imaging 2009: Image Processing, edited by Josien P. W. Pluim, Benoit M. Dawant,
Proc. of SPIE Vol. 7259, 72592U · © 2009 SPIE
CCC code: 1605-7422/09/$18 · doi: 10.1117/12.811181

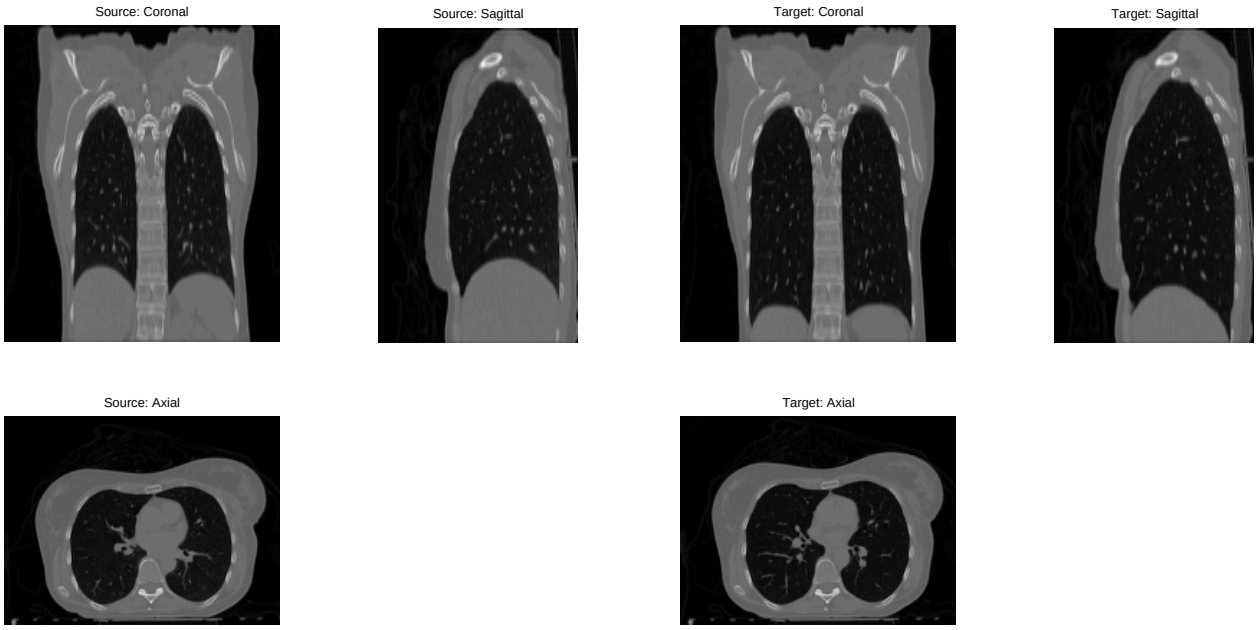

Figure 1. Coronal, sagittal and axial views of 3D exhale and inhale images of a real patient. Connectivity between diaphragm and rib bones is not preserved since diaphragm is sliding down while back rib bones remain at the similar locations.

applying both priors to respiratory motion estimation problem causes a conflict near the interface between rib cage and diaphragm area. Figure 1 shows that the connectivity between rib bones and diaphragm is not preserved due to sliding motion of diaphragm. This implies that enforcing invertibility alone will not be able to describe the motions of both diaphragm and rib bones. We will see experiment results in Section 3.

This paper proposes to use both a simple invertibility penalty[8,13] and a tissue rigidity penalty [10] and it also addresses the motion discontinuity near the interface between rib cage and diaphragm areas due to sliding motion. We relax a simple penalty that encourages local invertibility[8,13] by using a Geman-type function[14,15] so that the invertibility constraints can be reduced automatically around sliding area.

2. METHOD

2.1 Nonrigid image registration and local invertibility

A 3D nonrigid transformation $\underline{T}: \mathbf{R}^3 \rightarrow \mathbf{R}^3$ can be written

$$\underline{T}(\underline{r}) = \underline{r} + \underline{d}(\underline{r}), \tag{1}$$

where $\underline{r} = (x, y, z)$ and $\underline{d}(\underline{r})$ is the deformation. We model the 3D deformation $\underline{d} = (d^x, d^y, d^z)$ using a tensor product of nth-order B-splines

$$d^q(\underline{r}) = \sum_{i,j,k} c^q_{i,j,k} \beta\Big(\frac{x}{m_x} - i\Big)\beta\Big(\frac{y}{m_y} - j\Big)\beta\Big(\frac{z}{m_z} - k\Big), \tag{2}$$

where $q \in \{x, y, z\}$, β is a nth-order B-spline basis, and m_q are knot spacings. The goal in image registration is to estimate the deformation coefficients $\underline{c} = \{c^q_{i,j,k}\}$ by maximizing a similarity metric Ψ

$$\hat{\underline{c}} = \arg\max_{\underline{c}} \Psi[g(\cdot), f(\underline{T}(\cdot; \underline{c}))] \tag{3}$$

where $g(\underline{r})$ and $f(\underline{r})$ denote two 3D images. An unconstrained maximization in (3) will lead to physically implausible deformation estimates. We would like to constrain the transformation to be locally invertible. In principle, this could be

done by using the following "ideal" constraint set:

$$\underline{c} \in C_0 \equiv \{\underline{c} : \det \nabla \underline{T}(\underline{r}) > 0, \forall \underline{r}\}. \tag{4}$$

However, this constraint is hard to enforce so we relax this condition to have practical implementations . [2–8,13]

2.2 A simple penalty that encourages local invertibility

We recently proposed the following sufficient condition that ensures local invertibility. [8,13]

THEOREM 1. *Suppose* $0 \leq k_q < \frac{1}{2}$ *for* $q \in \{x, y, z\}$. *Define:*

$$\begin{aligned} C_4 \equiv \{\underline{c} :& -m_x k_x \leq c^x_{i+1,j,k} - c^x_{i,j,k} \leq m_x K_x, \\ & -m_y k_y \leq c^y_{i,j+1,k} - c^y_{i,j,k} \leq m_y K_y, \\ & -m_z k_z \leq c^z_{i,j,k+1} - c^z_{i,j,k} \leq m_z K_z, \\ & |c^q_{i+1,j,k} - c^q_{i,j,k}| \leq m_q k_q \text{ for } q = y, z, \\ & |c^q_{i,j+1,k} - c^q_{i,j,k}| \leq m_q k_q \text{ for } q = x, z, \\ & |c^q_{i,j,k+1} - c^q_{i,j,k}| \leq m_q k_q \text{ for } q = x, y, \quad \forall i, j, k\}. \end{aligned}$$

In (2), if $\underline{c} \in C_4$ *then the Jacobian determinant of* $\underline{T}$ *satisfies the bounds*

$$\begin{aligned} 1 - (k_x + k_y + k_z) \leq \det \nabla \underline{T}(\underline{r}) \leq (1 + K_x)(1 + K_y)(1 + K_z) \\ + (1 + K_x)k_y k_z + k_x(1 + K_y)k_z + k_x k_y(1 + K_z) \end{aligned}$$

for $\forall \underline{r} \in \mathbf{R}^3$. *Moreover, if* $k_x + k_y + k_z < 1$, *then the transformation (1) is locally invertible everywhere.*

Based on Theorem 1, we proposed the following simple penalty that encourages local invertibility:

$$R_I(\underline{c}) = \sum_{q \in \{x,y,z\}} \sum_{i,j,k} \left[p(c^q_{i+1,j,k} - c^q_{i,j,k}; \zeta^{q,x}_1, \zeta^{q,x}_2) + p(c^q_{i,j+1,k} - c^q_{i,j,k}; \zeta^{q,y}_1, \zeta^{q,y}_2) + p(c^q_{i,j,k+1} - c^q_{i,j,k}; \zeta^{q,z}_1, \zeta^{q,z}_2) \right] \tag{5}$$

where $\zeta^{q,s}_1 = -m_q k_q$ for $\forall s \in \{x, y, z\}$, $\zeta^{q,s}_2 = m_q k_q$ for $s \neq q$ and $\zeta^{q,s}_2 = m_q K_q$ for $s = q$. The function p is defined by

$$p(t; \zeta_1, \zeta_2) = \begin{cases} \frac{1}{2}(t - \zeta_1)^2, & t \leq \zeta_1 \\ 0, & \zeta_1 < t \leq \zeta_2 \\ \frac{1}{2}(t - \zeta_2)^2, & \text{otherwise.} \end{cases} \tag{6}$$

All parameters k_q, K_q are determined based on Theorem 1 and $k_x + k_y + k_z < 1$ allows (5) to be a penalty that encourages local invertibility. [8,13]

2.3 A tissue rigidity penalty

Staring *et al.*[11] and Modersitzki[12] defined a rigid transformation as follows.

DEFINITION 1. *A transformation* $\underline{T}(\underline{r})$ *is rigid if it is linear, i.e.,* $\partial^2_{i_1,i_2} \underline{T} = 0$ *for all* $i_1, i_2 \in \{x, y, z\}$, *orthogonal, i.e.,* $\nabla \underline{T}^T \nabla \underline{T} = I$, *and orientation preserving for* $\forall \underline{r} \in \mathbf{R}^3$, *i.e.,* $\det \nabla \underline{T} = 1$.

In this paper, we are applying an invertibility constraint together and in this case, orthogonal property implies orientation preserving. We also do not use linear property because it is computationally expensive (second order partial derivatives) and it does not seem to be a dominant term according to the experiment of Staring *et al.* [11] Therefore, we only use orthogonal property which is equivalent to Loeckxx *et al.* [9] and Ruan *et al.*[10] We use the following rigidity penalty function

$$R_R(\underline{c}) = \sum_{\underline{r}} \gamma(f(\underline{r})) ||\nabla \underline{T}(\underline{r})^T \nabla \underline{T}(\underline{r}) - I||^2_{Frob}, \tag{7}$$

where $|| \cdot ||_{Frob}$ is a Frobenius norm and $\gamma(x) = tanh((x - 1200)/10)/2 + 1/2$.

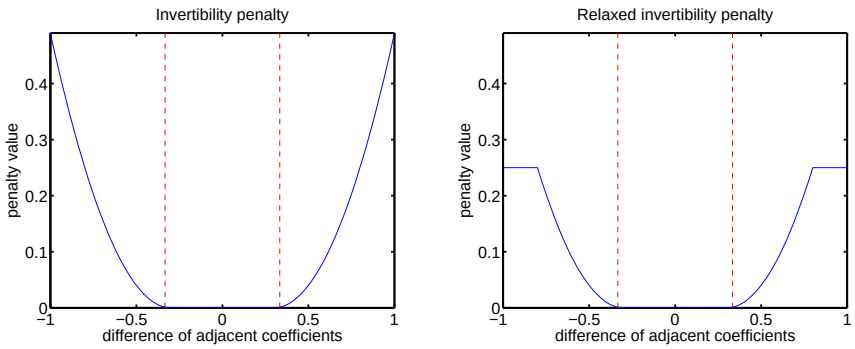

Figure 2. A quadratic-like penalty for invertibility constraint and a Geman-like penalty to relax invertibility constraint.

Ruan *et al.*[10] calculates the Jacobian values on all image voxels and Staring *et al.*[11] suggested to calculate only on all knot points instead of all image voxels. This choice depends on the scale of images. If a lower resolution image can capture the fine bone structure well, then we may calculate Jacobian values only on all knot points. However, if the original image has poor resolution, then we may have to get all Jacobian values on all image voxels. We may calculate only on image voxels whose γ function value is larger than a certain threshold value and it may lead to save lots of computation time since bones are very small proportion compared to the whole body.

2.4 A proposed penalty that considers sliding effects

In respiratory motion, sliding motion of diaphragm occurs mainly in the z-direction deformation and there are discontinuities along x- and y- directions of the z-direction deformation. Therefore, we relax only the invertibility penalty for x- and y- differences of z-direction deformation by using a Geman-type function so that it naturally accomodates the area of large differences between adjacent motion parameters. Specifically, we replace some of the $p(\cdot)$ terms in (5) as follows:

$$\begin{array}{lll} p(c^z_{i+1,j,k} - c^z_{i,j,k}; \zeta_1^{z,x}, \zeta_2^{z,x}) & to & g(c^z_{i+1,j,k} - c^z_{i,j,k}; \zeta_1^{z,x}, \zeta_2^{z,x}) \\ p(c^z_{i,j+1,k} - c^z_{i,j,k}; \zeta_1^{z,y}, \zeta_2^{z,y}) & to & g(c^z_{i,j+1,k} - c^z_{i,j,k}; \zeta_1^{z,y}, \zeta_2^{z,y}) \end{array} \tag{8}$$

where

$$g(t; \zeta_1, \zeta_2) = \begin{cases} \frac{1}{2}(\alpha_0 - \zeta_1)^2, & t \le \alpha_0 \\ \frac{1}{2}(t - \zeta_1)^2, & \alpha_0 < t \le \zeta_1 \\ 0, & \zeta_1 < t \le \zeta_2 \\ \frac{1}{2}(t - \zeta_2)^2, & \zeta_2 < t \le \alpha_1 \\ \frac{1}{2}(\alpha_1 - \zeta_2)^2, & \text{otherwise.} \end{cases} \tag{9}$$

Figure 2 depicts p and g functions.

2.5 Graduated non-convexity (GNC) method

Our proposed penalties change the problem in (3) as follows:

$$\hat{\underline{c}} = \arg\max_{\underline{c}} \Psi[g(\cdot), f(\underline{T}(\cdot; \underline{c}))] - \beta_I \tilde{R}_I(\underline{c}) - \beta_R R_R(\underline{c}) \tag{10}$$

where $\tilde{R}_I(\underline{c})$ is the modification of (5) according to (8). The proposed penalty function (9) is non-convex and it may cause local minima during the optimization. Blake *et al.* describe a graduated non-convexity method as an optimization method with Geman-type function.[15] It changes the shape of a function g from an almost convex function to a Geman function as optimization proceeds. We used a graduated non-convexity method combined with a conjugate gradient method to optimize the cost function (10).

Table 1. Negative Jacobian determinant values and data fitting RMS error

Method	# of (-) Jacobian determinant	Data fitting RMS error (HU)
No constraint	122597	30.59
Invertibility	0	36.26
Rigidity	0	38.13
Relaxed	341	38.11
Source	3145728	207.28

3. RESULTS

3.1 Experiment setup

We investigated $192 \times 128 \times 128$ 3D CT inhale and exhale images of a real patient shown in Figure 1. We used 3rd-order B-spline basis for deformation and deformation knots for every 4 voxels. Sum of squared difference was used for data fitting term. We did not use a multi-resolution for this experiment since lower resolution image seemed to lose detailed information about rib cage and our rigidity penalty did not seem to work well with poor resolution information. We performed 300 iterations with 4 cycles of GNC [15] and a conjugate gradient method.

3.2 Local invertibility and image matching

Figure 3 shows the deformed images for each method. No constraint case should be the best case in terms of matching deformed image to target image. The rest of the results of each method shows plausible deformed images. Table 1 shows these image matchings in a quantitative way. The data fitting RMS error of and between source and target images is 207.28 HU and no constraint case results in 30.59 HU after 300 iterations. However, It also results in 122597 voxel points of negative Jacobian determinant values among 3145728 voxels. Figure 4 shows projection views of these negative Jacobian determinants.

Applying invertibility penalty [8, 13] (Invertibility) alone and both invertibility and rigidity penalties (Rigidity) achieved 0 negative Jacobian determinant value. However, due to constraints applied, the data fidelity RMS error values are higher than no constraint case. Our proposed method (Relaxed) has 341 negative Jacobian determinant values among 3145728 voxels. This is natural because we intend to allow discontinuities near the interface between diaphragm and rib cage. Figure 4 (right) shows that the discontinuities appear near the area we intended in most of the cases. This method also achieved a better data fidelity RMS error value (38.11 HU) than Rigidity method (38.13 HU) since we relaxed an invertibility penalty.

3.3 Improved bone registration

Figure 3 (No constraint) shows a deformed image very close to an original target image. Bones near diaphragm in Invertibility case and Rigidity case show clear bone warps due to sliding motion of diaphragm. We chose rigidity penalty parameter according to our proposed method, so it is too weak to make bones corrected in the presence of strong invertibility penalty. The right side rib bone in coronal views went downward in both cases, and the spinal bones are stretched due to sliding effect. However, Figure 3 (Relaxed) shows that these bone moving / stretching are corrected. Figure 5 shows 3D bone structures for each method and shows that our proposed method corrects bone warps a lot compared to invertibility method or rigidity method.

3.4 Sliding effect

Figure 6 and 7 show quiver plots of deformations for each method in coronal and sagittal views. No constraint case shows very localized deformations. However, in the case of invertibility penalty, nearby deformation field was affected by major downward motion of diaphragm and we can even observe strong arrows outside the body or spine. However, our proposed method reduced the magnitude of arrows outside the body (and on rib bones) and on spine. It seems more realistic to have discontinuous motions near these areas.

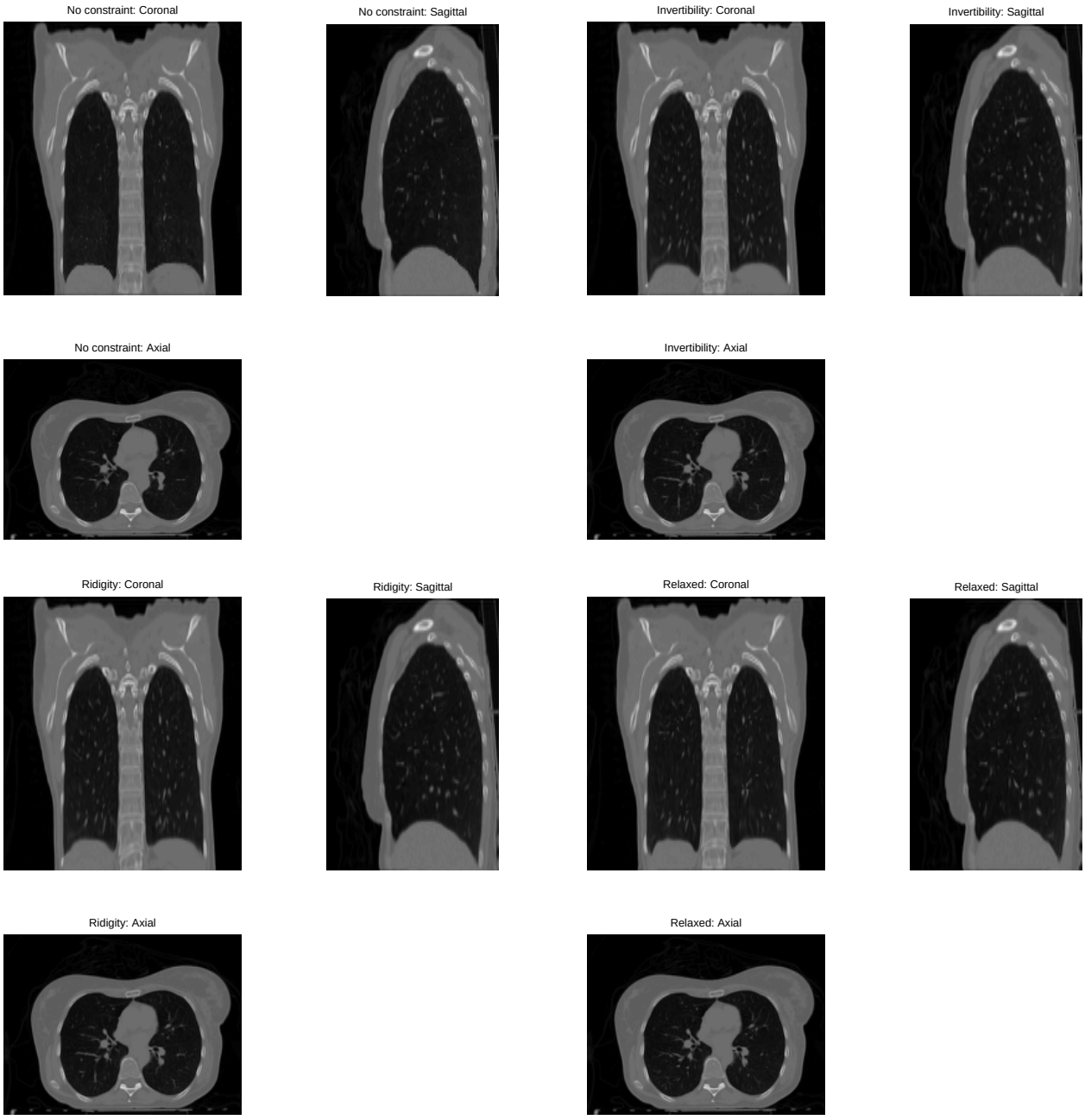

Figure 3. Coronal, sagittal and axial views of 3D deformed images with respect to each penalty: no constraint (top-left), invertibility (top-right), invertibility and rigidity (bottom-left), relaxed invertibility and rigidity (bottom-right).

4. DISCUSSION

This paper introduced a new relaxed invertibility penalty method as an extension of previous work. [8,13] We applied it to a 3D respiratory image registration problem with a rigidity penalty which corrected bone warps a lot with a small sacrifice of invertibility and data fidelity. Estimated deformation near diaphragm seems more realistic in terms of its discontinuity. However, due to the width of the support of cubic B-splines, cubic B-spline based image registration might not be the best way to implement tissue rigidity penalty. Rigid constraint near the support of this basis seems to lead less flexible

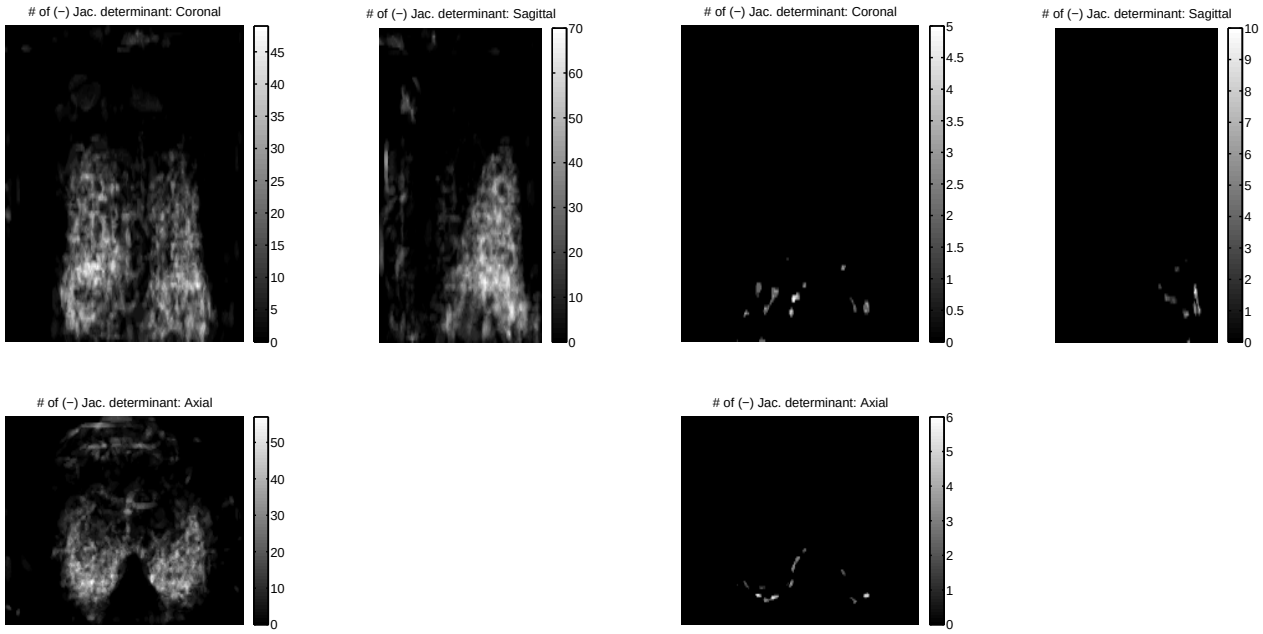

Figure 4. Projected coronal, sagittal and axial views of the number of non-positive Jacobian determinant values in no constraint and proposed method. Most of negative values in proposed method are near inbetween rib cage and diaphragm. Please note that the scales of each figure are different.

data fitting in the area of tissues near bones. More general settings in rigidity penalty [12] and in sliding treatment[16] seem a promising future work.

ACKNOWLEDGMENTS

The authors thank Dan Ruan for helpful discussion on sliding effects.

REFERENCES

[1] Crum, W. R., Hartkens, T., and Hill, D. L. G., "Non-rigid image registration: theory and practice," *The British Journal of Radiology* **77**, S140–S153 (2004).

[2] Kybic, J., Thévenaz, P., Nirkko, A., and Unser, M., "Unwarping of unidirectionally distorted EPI images," *IEEE Transactions on Medical Imaging* **19**, 80–93 (February 2000).

[3] Sdika, M., "A fast nonrigid image registration with constraints on the Jacobian using large scale constrained optimization," *IEEE Transactions on Medical Imaging* **27**, 271–281 (February 2008).

[4] Karacali, B. and Davatzikos, C., "Estimating topology preserving and smooth displacement fields," *IEEE Transactions on Medical Imaging* **23**(7), 868–880 (2004).

[5] Noblet, V., Heinrich, C., Heitz, F., and Armspach, J., "3-D deformable image registration: A topology preservation scheme based on hierarchical deformation models and interval analysis optimization," *IEEE Transactions on Image Processing* **14**(5), 553–566 (2005).

[6] Rohde, G. K., Aldroubi, A., and Dawant, B. M., "The adaptive bases algorithm for intensity-based nonrigid image registration," *IEEE Transactions on Medical Imaging* **22**(11), 1470–1479 (2003).

[7] Kim, J., *Intensity based image registration using robust similarity measure and constrained optimization: applications for radiation therapy*, PhD thesis, University of Michigan (2004).

[8] Chun, S. Y. and Fessler, J. A., "Regularized methods for topology-preserving smooth nonrigid image registration using b-spline basis," in [*Proc. IEEE Intl. Symp. Biomed. Imag.*], 1099 – 1102 (2008).

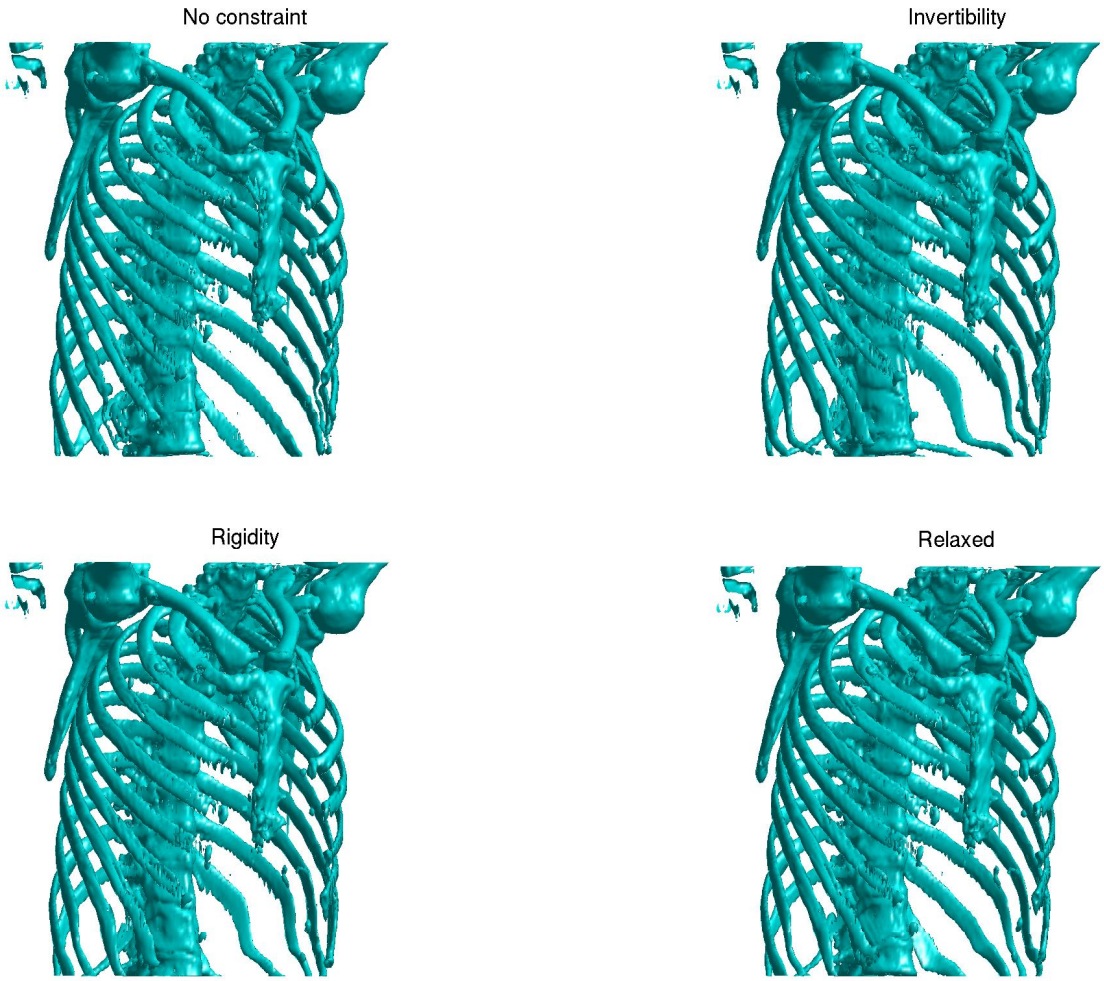

Figure 5. 3D bone structures of deformed images for No constraint, Invertibility, Rigidity , and Relaxed methods.

[9] Loeckx, D., Maes, F., Vandermeulen, D., and Suetens, P., "Nonrigid image registration using free-form deformations with a local rigidity constraint," in [*Medical Image Computing and Computer-Assisted Intervention*], **LNCS 3216**, 639–646 (2004).

[10] Ruan, D., Fessler, J. A., Roberson, M., Balter, J., and Kessler, M., "Nonrigid registration using regularization that accomodates local tissue rigidity," in [*Proc. of SPIE*], **6144**, 346–354 (2006).

[11] Staring, M., Klein, S., and Pluim, J. P. W., "A rigidity penalty term for nonrigid registration," *Med Phys.* **34**(11), 4098–4108 (2007).

[12] Modersitzki, J., "Flirt with rigidity–image registration with a local non-rigidity penalty," *Int. J. Comput. Vision* **76**(2), 153–163 (2008).

[13] Chun, S. Y. and Fessler, J. A., "A simple regularizer for B-spline nonrigid image registration that encourages local invertibility," *IEEE J. Sel. Top. Sig. Proc.* (2008). To appear.

[14] Geman, S. and Geman, D., "Stochastic relaxation, gibbs distributions, and the bayesian restoration of images," *IEEE Transactions on Pattern Analysis and Machine Intelligence* **6**(6), 721–742 (1984).

[15] Blake, A. and Zisserman, A., [*Visual Reconstruction*], MIT Press (1987).

[16] Ruan, D., Fessler, J. A., and Esedoglu, S., "Discontinuity preserving regularization for modeling sliding effects in medical image registration," in [*Proc. IEEE Nuc. Sci. Symp. Med. Im. Conf.*], (2008).

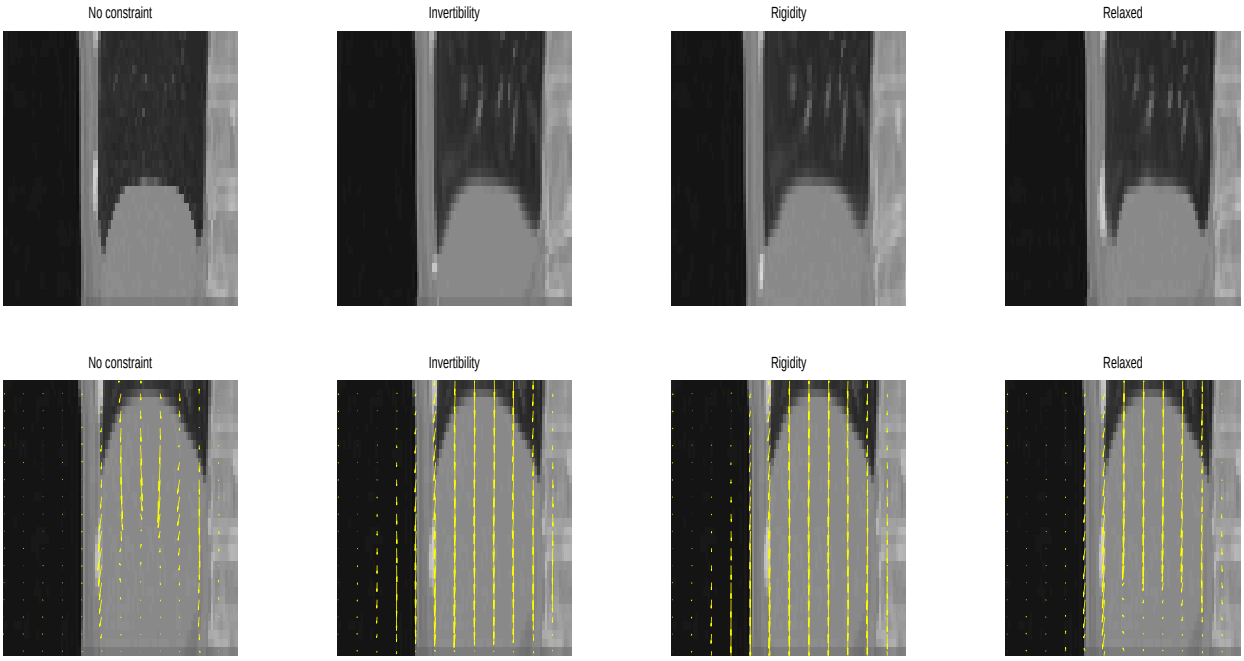

Figure 6. Zoomed coronal views of deformed images (TOP) by using no constraint, invertibility penalty (Invertibility), invertibility / rigidity penalty (Rigidity), and relaxed invertibility / rigidity penalty (Relaxed) and their quiver plots (BOTTOM).

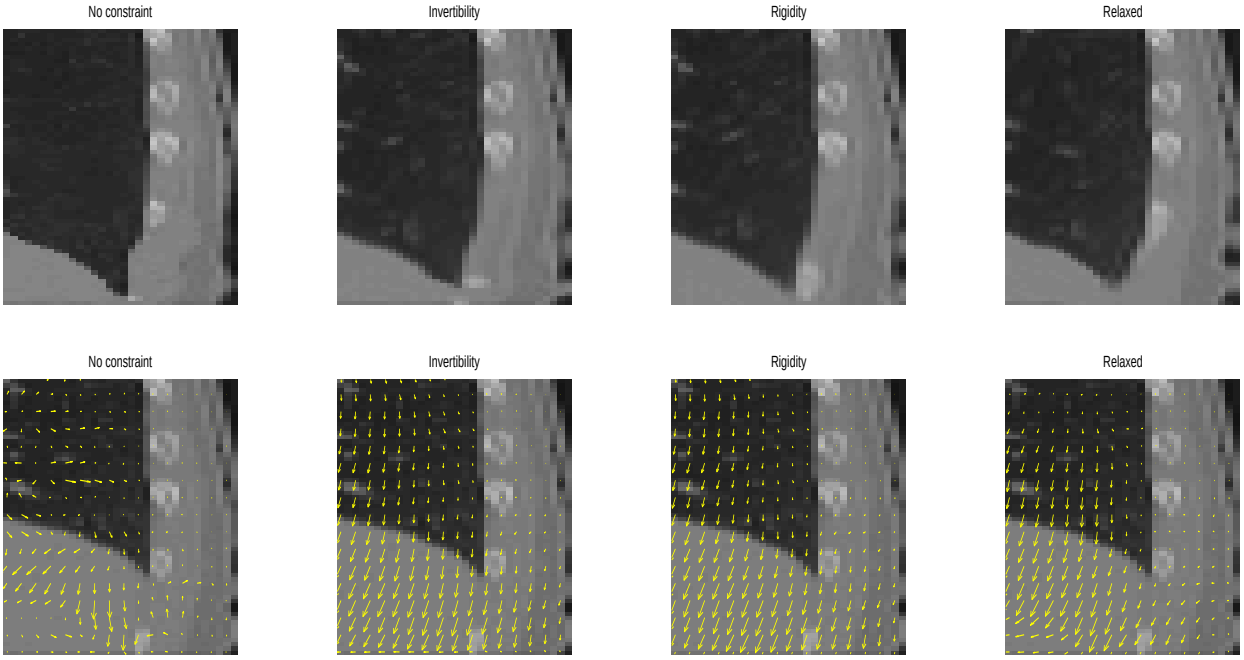

Figure 7. Zoomed sagittal views of deformed images (TOP) by using no constraint, invertibility penalty (Invertibility), invertibility / rigidity penalty (Rigidity), and relaxed invertibility / rigidity penalty (Relaxed) and their quiver plots (BOTTOM).